MIMO multirate feedforward controller design with selection of input multiplicities and intersample behavior analysis

Masahiro Mae*, Wataru Ohnishi, Hiroshi Fujimoto

The University of Tokyo, Japan

Abstract

Inversion-based feedforward control is a basic method of tracking controls. The aim of this paper is to design MIMO multirate feedforward controller that improves continuous-time tracking performance in MIMO LTI systems considering not only on-sample but also intersample behavior. Several types of MIMO multirate feedforward controllers are designed and evaluated in terms of the 2-norm of the control inputs. The approach is compared with a conventional MIMO single-rate feedforward controller in simulations. The approach improves the intersample behavior through the optimal selection of input multiplicities with MIMO multirate system inversion.

Keywords: Feedforward control, Inverse system, Multirate, Multi-input/multi-output systems, Digital control, Position control

1. Introduction

Inversion-based feedforward controllers play an important role in the tracking control of many high-precision mechatronic systems, such as wafer and LCD scanners, and industrial robots [1]. For the demands of high-performance, high-speed, and flexible tasks, many high-precision mechatronic systems have multiple degree-of-freedoms and are multi-input multi-output (MIMO) systems.

Many high-precision mechatronic systems are usually controlled by single-input single-output (SISO) controllers under the assumption that they are mechanically decoupled, and coupling problems between each axis can be ignored. Several high-precision mechatronic systems with severe coupling problem between each axis, such as a 6-degree-of-freedom high-precision positioning stage, are controlled with MIMO controllers, such as SISO controllers with a continuous-time pre-compensator [2], feedforward input shaping approach [3], and feedforward H_∞ approach [4]. However, these continuous-time controllers are usually discretized by Tustin transform for digital implementation. Therefore, the effect of discretization by the zero-order hold is not strictly considered and perfect tracking control cannot be achieved for a discrete-time nominal system.

In high-precision positioning systems with multiple actuators and sensors, such as a 6-degree-of-freedom high-precision positioning stage, it is common that the number of actuators and sensors are imaginarily converted by coordinate transformation to the same number of degrees of freedom of motion [2]. In this framework, this paper mainly focuses on MIMO linear-time-invariant (LTI) systems with an equal number of inputs and outputs. For the tracking control of MIMO LTI systems, MIMO feedforward controllers are needed to achieve good tracking performance by considering the coupling problems and redundancy of MIMO LTI systems.

The continuous-time inversion-based approaches such as [5, 6, 7] can be used for continuous-time systems. However, practical tracking controllers are often implemented by digital systems for large flexibility and low cost [8]. Therefore, the tracking control is conducted with digital control and has some limitations attributed to discretization. The main problem of the inversion-based feedforward controllers is the unstable discretized zeros, which are out of the unit circle on the z plane, of the controlled system discretized by a sampler and a holder. The inversion-based feedforward controllers are designed by the inverse of controlled systems and they have unstable poles due to the unstable zeros of the controlled systems.

To overcome the discretized unstable zero problems, several approximated inverse approaches are presented in the single-rate feedforward control, such as nonminimum-phase zeros ignore (NPZI) [9], zero-phase-error tracking control (ZPETC) [10] and zero-magnitude-error tracking controller (ZMETC) method [11]. However, these methods cannot achieve the exact tracking on sampling points because of the approximation.

An exact inverse approach, discrete-time stable inversion [12, 13], is presented, but this method cannot cope with the discretized zeros around $z = -1$ that become oscillating poles of the inversion-based feedforward controllers [14, 15]. It is noted that these single-rate feedforward control approaches can be extended to MIMO LTI systems [16, 17]. FIR filter tuning with a gradient approximation-based algorithm is presented for decoupling control of MIMO systems with a discrete-time controller [18]. However, this approach uses an optimization in the

*Corresponding author
Email address: mmae@ieee.org (Masahiro Mae)

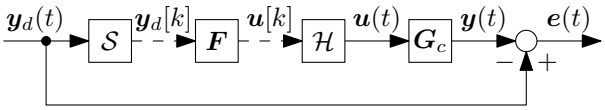

Figure 1: Block diagram of tracking control. The continuous-time system $\boldsymbol{G}_c$ is controlled by the discrete-time controller $\boldsymbol{F}$ with sampler $\mathcal{S}$ and holder $\mathcal{H}$. The objective is to minimize the continuous-time error $\boldsymbol{e}(t)$.

algorithm and it is not suitable when many kinds of references are used.

Based on these approaches in the single-rate feedforward control, a multirate control approach is presented [19]. Compared with the single-rate system, the multirate system has all zeros at $z = 0$. Therefore, the multirate feedforward controller has all poles at $z = 0$, and exact on-sample tracking can be achieved, and intersample behavior is also improved.

Previous researches show that the multirate feedforward control approach can be extended from the SISO LTI systems to the MIMO LTI systems [20]. MIMO multirate feedforward controller is effective to reject cross-couplings effects compared with the basic pre-compensator approach [21]. The MIMO multirate feedforward controller can be designed for several kinds because of the redundancy of MIMO LTI systems and multirate sampling periods. In this paper, a procedure of designing an optimal MIMO multirate feedforward controller is presented.

The outline of the paper is as follows. In Section 2, the problem of tracking with digital control is formulated. In Section 3, the conventional MIMO single-rate feedforward control approach and its limitations are presented before introducing the proposed method. In Section 4, the proposed MIMO multirate feedforward control approach is presented. In Section 5, the advantages of the approach are demonstrated by application to a MIMO motion system in the simulation. In Section 6, the conclusion of this paper is presented.

2. Problem formulation

In this section, the control problem is formulated. The overview of tracking control is shown in Figure 1.

2.1. Definition of multi-input multi-output system

The state equation and the output equation of an m-input m-output nth-order continuous-time linear time-invariant system $\boldsymbol{G}_c$ are given by

$$\dot{\boldsymbol{x}}(t) = \boldsymbol{A}_c\boldsymbol{x}(t) + \boldsymbol{B}_c\boldsymbol{u}(t), \tag{1}$$

$$\boldsymbol{y}(t) = \boldsymbol{C}_c\boldsymbol{x}(t), \tag{2}$$

$$\boldsymbol{B}_c = \begin{bmatrix} \boldsymbol{b}_{c_1} & \cdots & \boldsymbol{b}_{c_m} \end{bmatrix}, \quad \boldsymbol{C}_c = \begin{bmatrix} \boldsymbol{c}_{c_1} & \cdots & \boldsymbol{c}_{c_m} \end{bmatrix}^{\mathsf{T}},$$

where the state variables are $\boldsymbol{x}(t) \in \mathbb{R}^{n\times 1}$, inputs are $\boldsymbol{u}(t) \in \mathbb{R}^{m\times 1}$, outputs are $\boldsymbol{y}(t) \in \mathbb{R}^{m\times 1}$, and the matrices are $\boldsymbol{A}_c \in \mathbb{R}^{n\times n}$, $\boldsymbol{B}_c \in \mathbb{R}^{n\times m}$, and $\boldsymbol{C}_c \in \mathbb{R}^{m\times n}$. This paper mainly focuses on the MIMO LTI systems that have the same number of inputs and outputs. This is a natural assumption for mechatronic systems to achieve both the state controllability and the hardware cost reduction.

2.2. Discretization and sampling periods

The discrete-time system $\boldsymbol{G}_d$ discretized by the zero-order hold with $\boldsymbol{G}_c$ and the generalized sampling period δ is given by

$$\boldsymbol{x}[k+1] = \boldsymbol{A}_d\boldsymbol{x}[k] + \boldsymbol{B}_d\boldsymbol{u}[k], \tag{3}$$

$$\boldsymbol{y}[k] = \boldsymbol{C}_d\boldsymbol{x}[k], \tag{4}$$

where $k \in \mathbb{Z}$. $\boldsymbol{A}_d$, $\boldsymbol{B}_d$, and $\boldsymbol{C}_d$ are given by

$$\boldsymbol{A}_d = e^{\boldsymbol{A}_c\delta}, \quad \boldsymbol{B}_d = \int_0^\delta e^{\boldsymbol{A}_c\tau}\boldsymbol{B}_c \mathrm{d}\tau, \quad \boldsymbol{C}_d = \boldsymbol{C}_c. \tag{5}$$

In the discrete-time system, three sampling periods exist: T_r, T_y, and T_u, which represent the sampling periods of a reference $r(t)$, an output $y(t)$, and a control input $u(t)$, respectively. Three sampling periods T_r, T_y, and T_u are the same in the single-rate system and are different in the multirate system.

2.3. Perfect tracking control and intersample behavior

In the problem of tracking control, the discrete-time controller $\boldsymbol{F}$ should be designed as $\boldsymbol{G}_d\boldsymbol{F} = \boldsymbol{I}$, where $\boldsymbol{G}_d = \mathcal{S}\boldsymbol{G}_c\mathcal{H}$,at every sampling point and achieves perfect tracking control.

The perfect tracking control is defined as follows [10]:

Definition 1. *The perfect tracking control is defined as a method with which the plant output perfectly tracks the desired trajectory with zero tracking error at every sampling point.*

It is important that the perfect tracking control only guarantees the tracking error on the discrete-time sampling points, but not in the continuous-time. In the problem of tracking control, the objective is to minimize the continuous-time error $\boldsymbol{e}(t)$. Therefore, not only on-sample tracking error but also intersample tracking error should be considered in the design of the discrete-time controller $\boldsymbol{F}$.

In this paper, two types of discrete-time controllers are mentioned, the first is a single-rate feedforward controller and the second is a multirate feedforward controller.

3. Single-rate feedforward control for multi-input multi-output system

The single-rate system $\boldsymbol{G}_s$ discretized by the zero-order hold with $\boldsymbol{G}_c$ and the sampling period $\delta = T_u$ is given by

$$\boldsymbol{x}[k+1] = \boldsymbol{A}_s\boldsymbol{x}[k] + \boldsymbol{B}_s\boldsymbol{u}[k], \tag{6}$$

$$\boldsymbol{y}[k] = \boldsymbol{C}_s\boldsymbol{x}[k]. \tag{7}$$

From the state space representation of the single-rate system $\boldsymbol{G}_s$, control inputs $\boldsymbol{u}_{ff}[k]$ of the single-rate feedforward controller $\boldsymbol{F}_{sr}$ for the reference of the desired output trajectory $\boldsymbol{r}[k] = \boldsymbol{y}_d[k+1]$ are given by

$$\boldsymbol{u}_{ff}[k] = \boldsymbol{F}_{sr}\boldsymbol{y}_d[k+1], \tag{8}$$

where $\boldsymbol{F}_{sr}$ is given by

$$\boldsymbol{F}_{sr} = \left[\begin{array}{c|c} \boldsymbol{A}_s - \boldsymbol{B}_s(\boldsymbol{C}_s\boldsymbol{B}_s)^{-1}\boldsymbol{C}_s\boldsymbol{A}_s & \boldsymbol{B}_s(\boldsymbol{C}_s\boldsymbol{B}_s)^{-1} \\ \hline -(\boldsymbol{C}_s\boldsymbol{B}_s)^{-1}\boldsymbol{C}_s\boldsymbol{A}_s & (\boldsymbol{C}_s\boldsymbol{B}_s)^{-1} \end{array}\right]. \tag{9}$$

There is exact tracking of the desired output trajectory $\boldsymbol{y}_d$ at every sample in the systems with the single feedforward control.

However, the single-rate feedforward controller has a problem. It is known that a single-rate system discretized by the zero-order hold has discretized zeros depending on the relative order of the continuous-time system [22]. The discretized zeros appear around $z = -1$ on the real axis on the z plane. The single-rate feedforward controller is designed as the inverse of the single-rate system, and the zeros of the single-rate system become the poles of the single-rate feedforward controller. When the pole of the system is around $z = -1$ of the z plane, the system becomes oscillated or diverged. Therefore, the single-rate feedforward controller has the problem that the generated control inputs may be oscillated or diverged. If the single-rate feedforward controller F_{sr} has unstable poles, a stable inversion approach or an approximated inverse approach is used, see details in [12, 17].

On the other hand, the multirate feedforward controller is designed so that all poles are at $z = 0$ and the generated control inputs are not oscillated or diverged. In this paper, MIMO multirate feedforward controller is proposed to make the continuous-time error smaller than that of a MIMO single-rate feedforward controller.

4. Multirate feedforward control for multi-input multi-output system

In this section, the design method of the MIMO multirate feedforward controller is proposed for the tracking control of MIMO LTI systems. The multirate feedforward control has an advantage of intersample behavior compared with the single-rate feedforward control [13].

4.1. Design of input matrix from generalized controllability indices

The generalized controllability indices are defined as follows [20]:

Definition 2. *The generalized controllability indices of* $\boldsymbol{A}_c \in \mathbb{R}^{n\times n}$ *and* $\boldsymbol{B}_c = [\boldsymbol{b}_{c1}, \cdots, \boldsymbol{b}_{cm}] \in \mathbb{R}^{n\times m}$ *are defined as follows:*

$$\{\boldsymbol{b}_{c1}, \cdots, \boldsymbol{b}_{cm}, \boldsymbol{A}_c\boldsymbol{b}_{c1}, \cdots, \boldsymbol{A}_c\boldsymbol{b}_{cm}, \cdots, \boldsymbol{A}_c^{n-1}\boldsymbol{b}_{cm}\}.$$

If $(\boldsymbol{A}_c, \boldsymbol{B}_c)$ *is a controllable pair, n linearly independent vectors be selected from the he generalized controllability indices.*

The generalized controllability indices are the sets of the input multiplicities σ_l.

The input multiplicities σ_l is defined as follows [20]:

Definition 3. *Input multiplicities* σ_l *are defined as the number of the input which comes from the same input in the same frame period* T_f.

Setting φ as a set of n vectors selected from the generalized controllability indices, σ_l and N are defined by

$$\sigma_l = \text{number}\{k|\boldsymbol{A}_c^{k-1}\boldsymbol{b}_{cl} \in \varphi\}, \tag{10}$$

$$N = \max(\sigma_l), \tag{11}$$

where $l \in \mathbb{N}$ is the index of the inputs. The plant order n is equal to the sum of the input multiplicities σ_l as

$$\sum_{l=1}^{m} \sigma_l = n. \tag{12}$$

In MIMO LTI systems, n vectors are selected from the generalized controllability indices, and the full row rank matrix $\boldsymbol{B}$ can be designed for almost all discretized sampling periods[1]. Therefore, several types of multirate systems are designed according to the selection of input multiplicities.

From the selection of input multiplicities, T_{u_l}, which is the sampling period of lth input u_l, is defined by

$$T_{u_l} = \frac{N}{\sigma_l} T_u. \tag{13}$$

It is noted that the sampling period T_u is the smallest value of T_{u_l}.

A sampling period T_f is defined as the frame period which is the largest value between T_r, T_y and T_u. In this paper, the frame period T_f of the multirate system is defined by

$$T_f = T_r = NT_y = NT_u. \tag{14}$$

The multirate system $\boldsymbol{G}$ discretized by the zero-order hold with $\boldsymbol{G}_c$ and the sampling period $\delta = T_{u_l}$ is given by

$$\boldsymbol{x}[i+1] = \boldsymbol{A}\boldsymbol{x}[i] + \boldsymbol{B}\boldsymbol{u}[i], \tag{15}$$

$$\boldsymbol{y}[i] = \boldsymbol{C}\boldsymbol{x}[i], \tag{16}$$

where $i \in \mathbb{Z}$. $\boldsymbol{A}$, $\boldsymbol{B}$, $\boldsymbol{x}[i]$, and $\boldsymbol{u}[i]$ are given by

$$\boldsymbol{A} = e^{\boldsymbol{A}_c T_f}, \tag{17}$$

$$\boldsymbol{B} = \begin{bmatrix} \boldsymbol{B}_1 & \cdots & \boldsymbol{B}_l & \cdots & \boldsymbol{B}_m \end{bmatrix}, \tag{18}$$

$$\boldsymbol{C} = \boldsymbol{C}_c, \tag{19}$$

$$\boldsymbol{x}[i] = \boldsymbol{x}(iT_f), \tag{20}$$

$$\begin{aligned} \boldsymbol{u}[i] &= \begin{bmatrix} \boldsymbol{u}_1[i] & \cdots & \boldsymbol{u}_m[i] \end{bmatrix}^{\mathsf{T}} \\ &= \begin{bmatrix} u_{1_1}[i] & \cdots & u_{1_{\sigma_1}}[i] & u_{2_1}[i] & \cdots & u_{m_{\sigma_m}}[i] \end{bmatrix}^{\mathsf{T}}, \end{aligned} \tag{21}$$

and $\boldsymbol{B}_l$, $\boldsymbol{A}_{s_l}$ and $\boldsymbol{b}_{s_l}$ are defined as

$$\boldsymbol{B}_l = \begin{bmatrix} \boldsymbol{A}_{s_l}^{\sigma_l-1}\boldsymbol{b}_{s_l} & \boldsymbol{A}_{s_l}^{\sigma_l-2}\boldsymbol{b}_{s_l} & \cdots & \boldsymbol{A}_{s_l}\boldsymbol{b}_{s_l} & \boldsymbol{b}_{s_l} \end{bmatrix}, \tag{22}$$

$$\boldsymbol{A}_{s_l} = e^{\boldsymbol{A}_c T_{u_l}}, \quad \boldsymbol{b}_{s_l} = \int_0^{T_{u_l}} e^{\boldsymbol{A}_c \tau}\boldsymbol{b}_{c_l} \mathrm{d}\tau. \tag{23}$$

The input matrix $\boldsymbol{B}$ in a multirate system is designed by the generalized controllability indices depending on the input multiplicities σ_l. It becomes a nonsingular square matrix because of the definition of the generalized controllability indices. The state and input of the multirate system is shown in Figure 2.

[1] This is possible because the controllability of a continuous-time system is not preserved in the discrete system only if the two poles η_i and η_j have the same real parts, and the discretizing sampling period T satisfies $\eta_i = \eta_j + j\frac{2k\pi}{T}$ $(k = \pm 1, \pm 2, \ldots)$; furthermore, it is limited to only several cases [23].

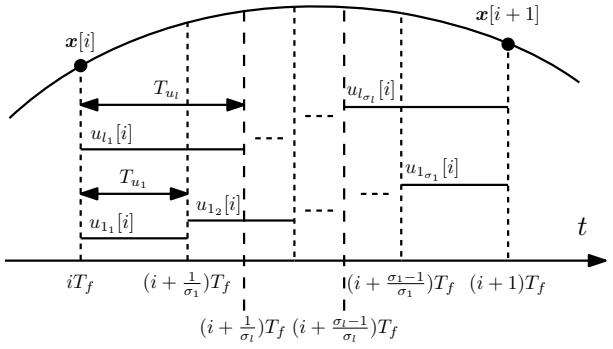

Figure 2: MIMO multirate input control.

4.2. Controller design and control input generation

From the state equation of the multirate system (15), control inputs $\boldsymbol{u}_{ff}[i]$ of the multirate feedforward controller $\boldsymbol{F}_{mr}$ for the reference of the desired state trajectory $\boldsymbol{r}[i] = \boldsymbol{x}_d[i+1]$ are given by

$$\boldsymbol{u}_{ff}[i] = \boldsymbol{F}_{mr}\boldsymbol{x}_d[i+1], \tag{24}$$

where $\boldsymbol{F}_{mr}$ and z is given by

$$\begin{aligned}\boldsymbol{F}_{mr} &= \boldsymbol{B}^{-1}(\boldsymbol{I} - z^{-1}\boldsymbol{A}) \\ &= \left[\begin{array}{c|c} \boldsymbol{O} & \boldsymbol{I} \\ \hline -\boldsymbol{B}^{-1}\boldsymbol{A} & \boldsymbol{B}^{-1} \end{array}\right], \qquad (25) \\ z &= e^{sT_f}. \qquad (26)\end{aligned}$$

There is exact tracking of the desired state trajectory $\boldsymbol{x}_d$ at every N samples in the nominal system with the multirate feedforward control. It is noted that all poles of the multirate feedforward controller $\boldsymbol{F}_{mr}$ are $z = 0$ because the state matrix of $\boldsymbol{F}_{mr}$ is $\boldsymbol{O}$, and smooth control input is generated compared with the single-rate feedforward controller $\boldsymbol{F}_{sr}$. For the details of the desired state trajectory generation, see [24, 25]. A block diagram of the control system is shown in Figure 3. L is a discrete-time lifting operator [8]. L^{-1} outputs the elements of the Nth dimensional vector $\boldsymbol{u}_{ff}[i]$, which are inputs at every period T_f, in the order from 1 to σ_l by T_{u_l}.

4.3. Optimal selection of input multiplicities

Several types of multirate feedforward controllers can be designed depending on the multirate system $\boldsymbol{G}$ with the selection of input multiplicities σ_l. There is exact tracking of the desired state trajectory $\boldsymbol{x}_d$ at every N samples in the systems with all kinds of multirate feedforward controllers [21]. However, the control inputs and intersample behavior are different depending on the multirate system $\boldsymbol{G}$. For the application of high-precision positioning control in mechatronic systems, continuous-time tracking error is preferred to be small, and also control input $\boldsymbol{u}$ should be smaller because of the limitation of mechatronic systems. An approach of designing the optimal MIMO multirate feedforward controller is proposed to make 2-norm of control inputs smaller in the rest of this section.

From the state equation of a multirate system (15), the part in which the control input $\boldsymbol{u}$ affects to the state $\boldsymbol{x}$ is given by

$$\boldsymbol{B}\boldsymbol{u}[i] = \boldsymbol{x}[i+1] - \boldsymbol{A}\boldsymbol{x}[i]. \tag{27}$$

In the multirate feedforward control, there is exact tracking of the state $\boldsymbol{x}[i]$ and $\boldsymbol{x}[i+1]$. The difference of the state $\boldsymbol{v}[i]$ is defined as

$$\boldsymbol{v}[i] = \boldsymbol{x}[i+1] - \boldsymbol{A}\boldsymbol{x}[i], \tag{28}$$

and the control input $\boldsymbol{u}[i]$ is represented as

$$\boldsymbol{u}[i] = \boldsymbol{B}^{-1}\boldsymbol{v}[i]. \tag{29}$$

The square of the 2-norm of the control input $\|\boldsymbol{u}[i]\|_2^2 = u_1^2 + \cdots + u_n^2$ is given by

$$\|\boldsymbol{u}[i]\|_2^2 = \boldsymbol{v}^{\mathsf{T}}[i](\boldsymbol{B}^{-1})^{\mathsf{T}}\boldsymbol{B}^{-1}\boldsymbol{v}[i], \tag{30}$$

and $\|\boldsymbol{u}[i]\|_2^2$ becomes a quadratic form of $\boldsymbol{v}[i]$.

For the normalization of the difference of the state, $\boldsymbol{v}[i]$ is defined as the unit sphere:

$$\|\boldsymbol{v}[i]\|_2^2 = v_1^2 + \cdots + v_n^2 = 1. \tag{31}$$

According to the relationship between the range of a quadratic form with the unit sphere and eigenvalues [26], the range of $\|\boldsymbol{u}[i]\|_2^2$ is given by

$$\lambda_n \le \|\boldsymbol{u}[i]\|_2^2 \le \lambda_1 \quad (\lambda_n \le \lambda_{(n-1)} \le \cdots \le \lambda_1), \tag{32}$$

where λ_i is the eigenvalue of $(\boldsymbol{B}^{-1})^{\mathsf{T}}\boldsymbol{B}^{-1}$. λ_{ci}, which is the eigenvalue of $\boldsymbol{B}\boldsymbol{B}^{\mathsf{T}}$, is the reciprocal of λ_i as

$$\lambda_{ci} = \frac{1}{\lambda_i}, \tag{33}$$

and the range of $\|\boldsymbol{u}[i]\|_2^2$ given by

$$\frac{1}{\lambda_{cn}} \le \|\boldsymbol{u}[i]\|_2^2 \le \frac{1}{\lambda_{c1}} \quad (\lambda_{c1} \le \lambda_{c2} \le \cdots \le \lambda_{cn}). \tag{34}$$

σ_{ci}, which is the singular value of the input matrix $\boldsymbol{B}$ is the square root of λ_{ci} as

$$\sigma_{ci}(\boldsymbol{B}) = \sqrt{\lambda_{ci}(\boldsymbol{B}\boldsymbol{B}^{\mathsf{T}})}, \tag{35}$$

and the range of 2-norm of the control input $\|\boldsymbol{u}[i]\|_2$ is given by

$$\frac{1}{\sigma_{cn}} \le \|\boldsymbol{u}[i]\|_2 \le \frac{1}{\sigma_{c1}} \quad (\sigma_{c1} \le \sigma_{c2} \le \cdots \le \sigma_{cn}). \tag{36}$$

If 2-norm of the control input $\|\boldsymbol{u}[i]\|_2$ is too large, it is not suitable for the limitation of the mechatronic systems. Making the upper bound of the 2-norm of control input $\|\boldsymbol{u}[i]\|_2$ smaller is equal making the smallest singular value $\sigma_{c1}(\boldsymbol{B})$ larger. From this consideration, the input multiplicity is selected so that the smallest singular value $\sigma_{c1}(\boldsymbol{B})$ becomes the largest. Therefore, the optimal design of the MIMO multirate feedforward controller to make the maximum value of 2-norm of control inputs smaller is proposed. The MIMO multirate feedforward controller cannot specify the band of the continuous-time error because it only guarantees the exact tracking of the desired state trajectory $\boldsymbol{x}_d$ at every frame period T_f in the nominal system, but the intersample behavior becomes smoothly connected between the discrete sampling points in continuous time with the control inputs of the optimally designed controller. The analysis of the bound of the continuous-time error is an open issue.

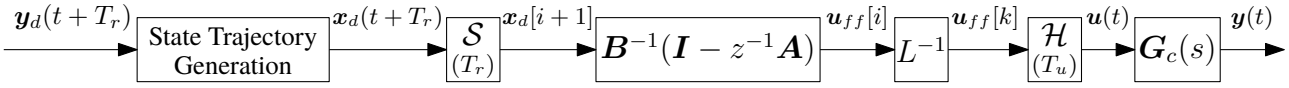

Figure 3: Block diagram of MIMO multirate feedforward control. $\mathcal{S}$, $\mathcal{H}$, and L denote sampler, holder, and lifting operator [8], respectively. z and z_s denote e^{sT_r} and e^{sT_u}, respectively.

4.4. Example: intersample behavior of multirate feedforward in different sets of input multiplicities

The optimal design of the MIMO multirate feedforward controller is validated with the example of a numerical simulation.

The continuous-time system $\boldsymbol{G}_c$ is defined as the transfer function matrix (37). The reference of the desired output trajectory $\boldsymbol{y}_d$ is given by 7th-order polynomials which change from 0 to 1 in 0 s to 400 µs for each output. The sampling period of the control input is set to $T_u = 400\,\mu\text{s}$. For the design of MIMO multirate feedforward controller, seven types of sets of input multiplicities are selected as

$$(\sigma_1, \sigma_2) = (0,6), (1,5), (2,4), (3,3), (4,2), (5,1), (6,0). \quad (38)$$

The examples of multirate inputs are shown in Figure 5.

The smallest singular value $\sigma_{c1}(\boldsymbol{B})$ and the simulation results are shown in Table 1. From the procedure of designing the optimal MIMO multirate feedforward controller, the set of input multiplicities in which the smallest singular value $\sigma_{c1}(\boldsymbol{B})$ is the largest is the optimal set of input multiplicities for the controlled system. The advantage of this procedure is that the optimal MIMO multirate feedforward controller is designed without numerical simulations. When the order of the system is high or the number of inputs and outputs is large, the number of the set of input multiplicities becomes enormous. Therefore, testing all sets with several references in numerical simulations spends a large amount of time, and the proposed design procedure is effective.

The validity of the procedure can be confirmed from the root mean square and the maximum absolute value of control inputs $\boldsymbol{u}$ and tracking errors $\boldsymbol{e}$ in Table 1. The trend is that control inputs $\boldsymbol{u}$ and tracking errors $\boldsymbol{e}$ become small when the smallest singular value $\sigma_{c1}(\boldsymbol{B})$ is large. From Table 1, the optimal MIMO multirate feedforward controller is designed with the set of input multiplicities $(\sigma_1, \sigma_2) = (4,2)$ which makes the smallest singular value $\sigma_{c1}(\boldsymbol{B})$ largest, and the root mean square of tracking errors $\boldsymbol{e}$ are the smallest in all sets.

In summary, the proposed procedure is validated, and the optimal MIMO multirate feedforward controller can be designed with the set of input multiplicities which makes the smallest singular value $\sigma_{c1}(\boldsymbol{B})$ largest, without spending time on numerical simulations.

5. Verification in multi-input multi-output positioning system

In this section, the tracking performance considering the intersample behavior of the optimal MIMO multirate feedforward controller is verified compared with that of a MIMO single-rate feedforward controller.

5.1. System modeling

The approach is validated on the two-inertia system motor bench shown in Figure 6(a). The two-inertia system motor bench has two motors on the left and right side and two motors are connected by the flexible shaft as shown in Figure 6(b). The two-inertia system motor bench is used for theoretical and applicability validation. The two-inertia system motor bench has 20 bit/rev optical encoder for both sides which is enough high resolution for high-precision mechatronic systems. In this paper, the two-inertia system motor bench is modeled as a two-input two-output 4th-order system. The block diagram of the system is shown in Figure 7. The two inputs $\boldsymbol{u}$ are the left and right side torque, τ_l and τ_r, and the outputs $\boldsymbol{y}$ are the left and right side angle, θ_l and θ_r, respectively. The Bode diagram of a frequency response function measurement of the system is shown in Figure 8. The measurement is obtained through the identification experiment with a multisine input [27] from 1 Hz to 1249 Hz, and a sampling frequency is 2.5 kHz. From the frequency response function measurement, the parameters of the two-inertia system motor bench are given as shown in Table 2 and the identified continuous-time system $\boldsymbol{G}_c$ is given by the state space model with the state equation (39) and the output equation (40).

$$\frac{\mathrm{d}}{\mathrm{d}t}\begin{bmatrix}\theta_l(t)\\ \dot{\theta}_l(t)\\ \theta_r(t)\\ \dot{\theta}_r(t)\end{bmatrix} = \begin{bmatrix}0 & 1 & 0 & 0\\ -\frac{K}{J_l} & -\frac{D_l}{J_l} & \frac{K}{J_l} & 0\\ 0 & 0 & 0 & 1\\ \frac{K}{J_r} & 0 & -\frac{K}{J_r} & -\frac{D_r}{J_r}\end{bmatrix}\begin{bmatrix}\theta_l(t)\\ \dot{\theta}_l(t)\\ \theta_r(t)\\ \dot{\theta}_r(t)\end{bmatrix} + \begin{bmatrix}0 & 0\\ \frac{1}{J_l} & 0\\ 0 & 0\\ 0 & \frac{1}{J_r}\end{bmatrix}\begin{bmatrix}\tau_l(t)\\ \tau_r(t)\end{bmatrix} \quad (39)$$

$$\begin{bmatrix}\theta_l(t)\\ \theta_r(t)\end{bmatrix} = \begin{bmatrix}1 & 0 & 0 & 0\\ 0 & 0 & 1 & 0\end{bmatrix}\begin{bmatrix}\theta_l(t)\\ \dot{\theta}_l(t)\\ \theta_r(t)\\ \dot{\theta}_r(t)\end{bmatrix} \quad (40)$$

5.2. Conditions

The conventional MIMO single-rate feedforward controller $\boldsymbol{F}_{sr}$ and the proposed MIMO multirate feedforward controller $\boldsymbol{F}_{mr}$ are compared in the tracking control of the continuous-time system $\boldsymbol{G}_c$. With the proposed procedure, the optimal MIMO multirate feedforward controller is designed for $\boldsymbol{G}_c$ with the set of input multiplicities $(\sigma_1, \sigma_2) = (2,2)$ which makes the smallest singular value $\sigma_{c1}(\boldsymbol{B})$ largest. The poles and zeros of the feedforward controllers $\boldsymbol{F}_{sr}$ and $\boldsymbol{F}_{mr}$ are shown in Figure 9. From Figure 9(a), the conventional MIMO single-rate feedforward controller $\boldsymbol{F}_{sr}$ has one pole around $z = -1$ which leads to an oscillation, and from Figure 9(b), the proposed MIMO multirate feedforward controller $\boldsymbol{F}_{mr}$ has all poles on $z = 0$. The reference of the desired output trajectory $\boldsymbol{y}_d$ is given by 7th-order polynomials which change from 0 to 100 µrad in 0.8 ms to 2 ms for each output. The sampling period of the control input is set to $T_u = 400\,\mu\text{s}$. From these conditions, the reference signal is steep enough compared with T_u.

$$\boldsymbol{G}_c(s) = \frac{1}{s^6 + 8895s^5 + 3.979\times10^7 s^4 + 2.428\times10^9 s^3 + 9.099\times10^{12} s^2 + 4.382\times10^{13} s + 24} \begin{bmatrix} 4.702\times10^{10}s^2 + 2.294\times10^{11}s + 5.477\times10^{15} & 1.387\times10^8 s^2 + 1.233\times10^{12}s + 5.477\times10^{15} \\ 5.477\times10^{15} & 1220s^4 + 1.085\times10^7 s^3 + 4.835\times10^{10}s^2 + 1.462\times10^{12}s + 5.477\times10^{15} \end{bmatrix} \tag{37}$$

Table 1: $\sigma_{c1}(\boldsymbol{B})$, the smallest singular value of $\boldsymbol{B}$, and root mean square and maximum absolute value of control inputs $\boldsymbol{u}$ and tracking errors $\boldsymbol{e}$ depending on sets of input multiplicities (σ_1, σ_2).

(σ_1,σ_2)	$\sigma_{c1}(\boldsymbol{B})$	RMS(u_1)	MAX($\lvert u_1\rvert$)	RMS(u_2)	MAX($\lvert u_2\rvert$)	RMS(e_1)	MAX($\lvert e_1\rvert$)	RMS(e_2)	MAX($\lvert e_2\rvert$)
$(0,6)$	1.86×10^{-16}	0.00×10^{00}	0.00×10^{00}	9.81×10^{04}	2.27×10^{05}	4.48×10^{-01}	9.94×10^{-01}	7.34×10^{00}	1.53×10^{01}
$(1,5)$	6.77×10^{-13}	5.54×10^{-12}	7.83×10^{-12}	1.71×10^{05}	4.27×10^{05}	4.01×10^{-01}	9.88×10^{-01}	9.30×10^{00}	2.47×10^{01}
$(2,4)$	8.09×10^{-07}	2.24×10^{-10}	5.01×10^{-10}	3.95×10^{05}	8.37×10^{05}	3.28×10^{-01}	9.70×10^{-01}	1.40×10^{01}	3.67×10^{01}
$(3,3)$	4.70×10^{-07}	4.70×10^{03}	1.48×10^{04}	6.72×10^{05}	1.73×10^{06}	2.26×10^{-01}	8.50×10^{-01}	4.01×10^{01}	1.28×10^{02}
$(4,2)$	1.54×10^{-04}	2.06×10^{03}	4.78×10^{03}	8.12×10^{02}	1.29×10^{03}	2.77×10^{-01}	9.20×10^{-01}	3.09×10^{-01}	8.99×10^{-01}
$(5,1)$	5.70×10^{-07}	5.84×10^{05}	1.51×10^{06}	2.27×10^{03}	3.21×10^{03}	3.44×10^{01}	1.01×10^{02}	7.66×10^{-01}	1.70×10^{00}
$(6,0)$	1.01×10^{-06}	3.44×10^{05}	7.45×10^{05}	0.00×10^{00}	0.00×10^{00}	1.05×10^{01}	2.58×10^{01}	4.11×10^{-01}	9.96×10^{-01}

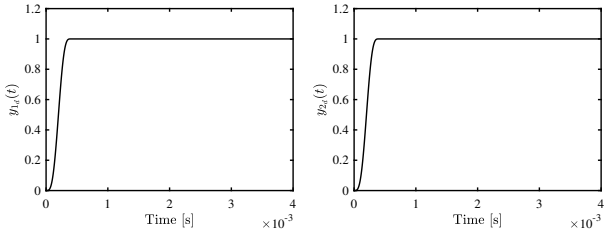

(a) $y_{1_d}(t)$ (b) $y_{2_d}(t)$

Figure 4: Desired output trajectory $\boldsymbol{y}_d(t) = [y_{1_d}(t)\ y_{2_d}(t)]^{\mathsf{T}}$: they are 7th-order polynomials, respectively.

Table 2: Parameters of two-inertia system motor bench.

J_l	$8.40\times10^{-4}\,\mathrm{kgm^2}$	J_r	$8.20\times10^{-4}\,\mathrm{kgm^2}$
D_l	$4.00\times10^{-3}\,\mathrm{Nms/rad}$	D_r	$4.00\times10^{-3}\,\mathrm{Nms/rad}$
K	$95.5\,\mathrm{Nm/rad}$		

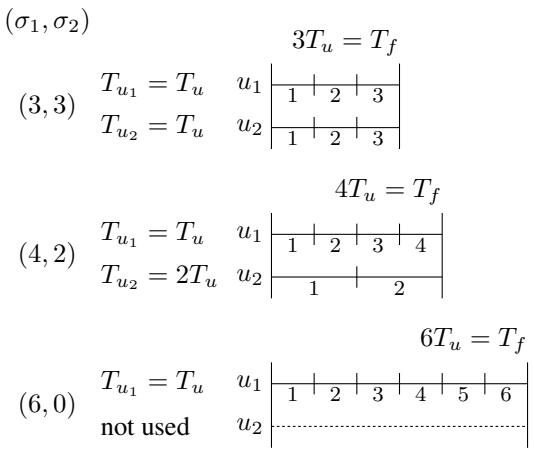

Figure 5: Examples of multirate inputs. Two inputs u_1 and u_2 are generated according to the input multiplicities (σ_1, σ_2). A control input with 0 input multiplicity is not in use.

5.3. Results: intersample behavior of multirate feedforward and single-rate feedforward

The simulation results are shown in Figure 10. Figure 10(a) and Figure 10(b) show that the control inputs of the conventional MIMO single-rate feedforward controller $\boldsymbol{F}_{sr}$ oscillate and the proposed MIMO multirate feedforward controller $\boldsymbol{F}_{mr}$ generates the smooth control inputs. Figure 10(c) and Figure 10(d) show that the outputs of the single-rate feedforward controller are oscillated because of the oscillated control inputs, and the outputs of the multirate feedforward controller are settled after 2 s. Figure 10(e) and Figure 10(f) show that the continuous-time tracking error of the multirate feedforward controller is smaller than that of the single-rate feedforward controller, thus the effectiveness proposed method is verified.

MIMO multirate feedforward controller is used in the two-degree-of-freedom robust control with feedback controllers which reduce modeling error and disturbances. The role of the feedforward controller is the nominal tracking performance in the two-degree-of-freedom control scheme, and the simulation validations accurately verify it. In summary, the proposed optimal MIMO multirate feedforward controller outperforms the conventional MIMO single-rate feedforward controller in smooth control inputs and continuous-time tracking errors.

6. Conclusion

The procedure of the optimal MIMO multirate feedforward controller design is proposed. The optimal MIMO multirate feedforward controller makes the upper bound of the 2-norm of control input $\|\boldsymbol{u}[i]\|_2$ smaller, and as a result, the continuous-time tracking errors become smaller. The numerical simulation is conducted for the 6th-order system, and the proposed procedure of the selection of input multiplicities is validated.

The continuous-time tracking errors of the proposed MIMO multirate feedforward controller $\boldsymbol{F}_{mr}$ are compared with the conventional MIMO single-rate feedforward controller $\boldsymbol{F}_{sr}$ with the two-inertia system motor bench. Depending on the poles of each controller, the conventional single-rate controller generates oscillated control inputs and the proposed multirate controller generates smooth control inputs. As a result, continuous-time tracking errors of the multirate controller are better than that of the single-rate controller in the MIMO LTI system.

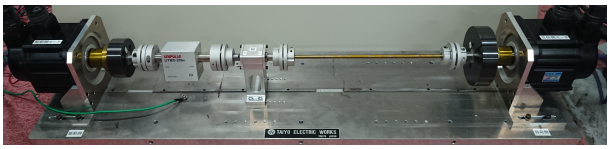

(a) Photograph of two-inertia system motor bench.

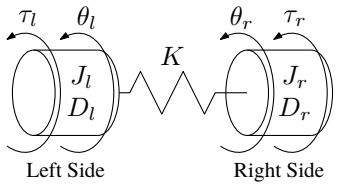

(b) Model of two-inertia system.

Figure 6: Details of two-inertia system motor bench. In this paper, the two-inertia system motor bench is modeled as a two-input two-output system. The two inputs are left side torque τ_l and right side torque τ_r, respectively. The two outputs are left side angle θ_l and right side angle θ_r, respectively.

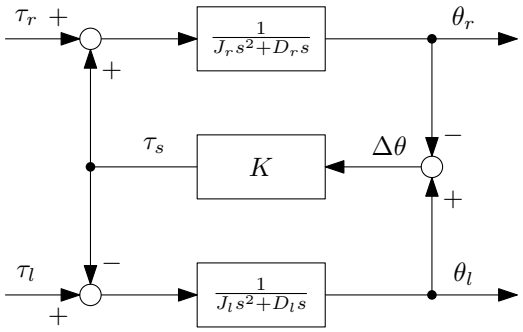

Figure 7: Block diagram of two-inertia system.

Ongoing research focuses on MIMO LTI systems which have a different number of inputs and outputs, and the combination of single-rate and multirate controllers.

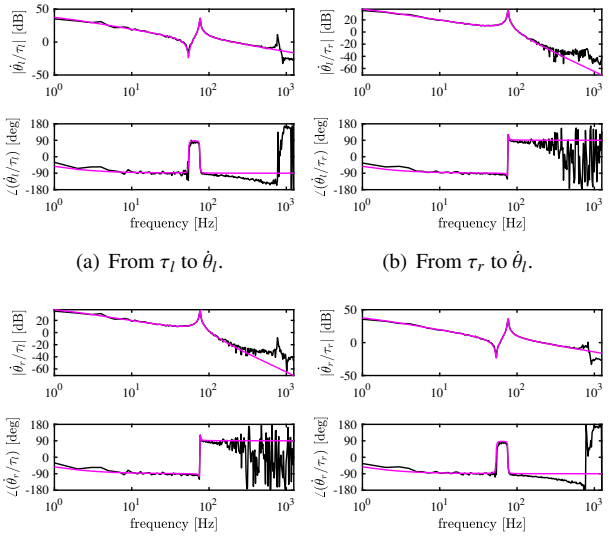

(a) From τ_l to $\dot{\theta}_l$. (b) From τ_r to $\dot{\theta}_l$.

(c) From τ_l to $\dot{\theta}_r$. (d) From τ_r to $\dot{\theta}_r$.

Figure 8: Bode diagram of two-inertia system motor bench. The black line is a frequency response function measurement of the system and the magenta line is the identified continuous-time system.

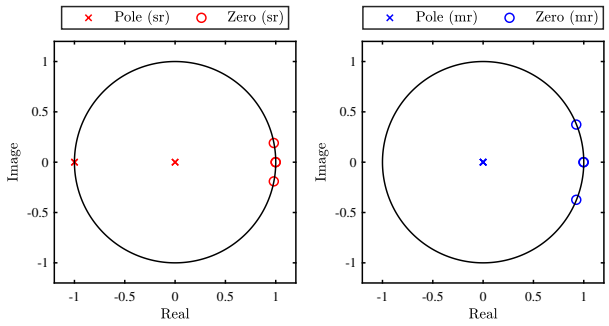

(a) $\boldsymbol{F}_{sr}$ (b) $\boldsymbol{F}_{mr}$

Figure 9: Poles and zeros of multirate feedforward controller $\boldsymbol{F}_{mr}$ and single-rate feedforward controller $\boldsymbol{F}_{sr}$ with unit circle on z plane.

References

[1] T. Oomen, Advanced Motion Control for Precision Mechatronics: Control, Identification, and Learning of Complex Systems, IEEJ Journal of Industry Applications 7 (2) (2018) 127–140. doi:10.1541/ieejjia.7.127.

[2] H. Butler, Position Control in Lithographic Equipment [Applications of Control], IEEE Control Systems 31 (5) (2011) 28–47. doi:10.1109/MCS.2011.941882.

[3] Y. Al Hamidi, M. Rakotondrabe, Multi-Mode Vibration Suppression in MIMO Systems by Extending the Zero Placement Input Shaping Technique: Applications to a 3-DOF Piezoelectric Tube Actuator, Actuators 5 (2) (2016) 13. doi:10.3390/act5020013.

[4] D. Habineza, M. Zouari, Y. Le Gorrec, M. Rakotondrabe, Multivariable Compensation of Hysteresis, Creep, Badly Damped Vibration, and Cross Couplings in Multiaxes Piezoelectric Actuators, IEEE Transactions on Automation Science and Engineering 15 (4) (2018) 1639–1653. doi:10.1109/TASE.2017.2772221.

[5] L. Hunt, G. Meyer, R. Su, Noncausal inverses for linear systems, IEEE Transactions on Automatic Control 41 (4) (1996) 608–611. doi:10.1109/9.489285.

[6] S. Devasia, Degang Chen, B. Paden, Nonlinear inversion-based output tracking, IEEE Transactions on Automatic Control 41 (7) (1996) 930–942. doi:10.1109/9.508898.

[7] T. Sogo, On the equivalence between stable inversion for nonminimum phase systems and reciprocal transfer functions defined by the two-sided Laplace transform, Automatica 46 (1) (2010) 122–126. doi:10.1016/j.automatica.2009.10.008.

[8] T. Chen, B. A. Francis, Optimal Sampled-Data Control Systems, Springer London, London, 1995. arXiv:arXiv:1011.1669v3, doi:10.1007/978-1-4471-3037-6.

[9] J. Butterworth, L. Pao, D. Abramovitch, Analysis and comparison of three discrete-time feedforward model-inverse control techniques for nonminimum-phase systems, Mechatronics 22 (5) (2012) 577–587. doi:10.1016/j.mechatronics.2011.12.006.

[10] M. Tomizuka, Zero Phase Error Tracking Algorithm for Digital Control, Journal of Dynamic Systems, Measurement, and Control 109 (1) (1987) 65. doi:10.1115/1.3143822.

[11] J. Wen, B. Potsaid, An experimental study of a high performance motion control system, in: Proceedings of the 2004 American Control Conference, Vol. 6, IEEE, 2004, pp. 5158–5163. doi:10.23919/ACC.2004.1384671.

[12] J. van Zundert, T. Oomen, On inversion-based approaches for feedforward and ILC, Mechatronics 50 (November 2016) (2018) 282–291. doi:10.1016/j.mechatronics.2017.09.010.

[13] J. Van Zundert, W. Ohnishi, H. Fujimoto, T. Oomen, Improving Inter-sample Behavior in Discrete-Time System Inversion: With Application to LTI and LPTV Systems, IEEE/ASME Transactions on Mechatronics

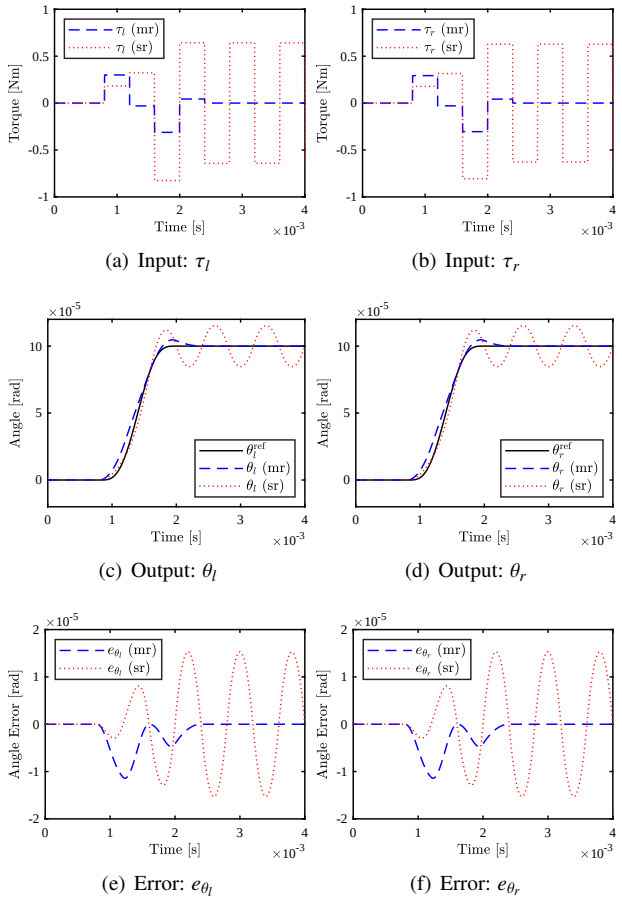

(a) Input: τ_l (b) Input: τ_r

(c) Output: θ_l (d) Output: θ_r

(e) Error: e_{θ_l} (f) Error: e_{θ_r}

Figure 10: Simulation results of multirate and single-rate feedforward control.

PP (c) (2019) 1–1. doi:10.1109/TMECH.2019.2953829.

[14] K. L. Moore, S. Bhattacharyya, M. Dahleh, Capabilities and limitations of multirate control schemes, Automatica 29 (4) (1993) 941–951. doi:10.1016/0005-1098(93)90098-E.

[15] T. Sogo, M. Joo, Design of Compensators to Relocate Sampling Zeros of Digital Control Systems for DC Motors, SICE Journal of Control, Measurement, and System Integration 5 (5) (2012) 283–289. doi:10.9746/jcmsi.5.283.

[16] K. George, M. Verhaegen, J. M. a. Scherpen, Stable Inversion of MIMO Linear Discrete Time Non-Minimum Phase Systems, in: Proceedings of the 7th Mediterranean Conference on Control and Automation, 1999, pp. 267–281.

[17] L. Blanken, T. Oomen, Multivariable Iterative Learning Control Design Procedures: From Decentralized to Centralized, Illustrated on an Industrial Printer, IEEE Transactions on Control Systems Technology (2019) 1–8arXiv:1806.08550, doi:10.1109/TCST.2019.2903021.

[18] M. Heertjes, D. Hennekens, M. Steinbuch, MIMO feed-forward design in wafer scanners using a gradient approximation-based algorithm, Control Engineering Practice 18 (5) (2010) 495–506. doi:10.1016/j.conengprac.2010.01.006.

[19] H. Fujimoto, Y. Hori, A. Kawamura, Perfect tracking control based on multirate feedforward control with generalized sampling periods, IEEE Transactions on Industrial Electronics 48 (3) (2001) 636–644. doi:10.1109/41.925591.

[20] H. Fujimoto, General Framework of Multirate Sampling Control and Applications to Motion Control Systems, Doctoral Dissertation.

[21] M. Mae, W. Ohnishi, H. Fujimoto, Y. Hori, Perfect Tracking Control Considering Generalized Controllability Indices and Application for High-Precision Stage in Translation and Pitching, IEEJ Journal of Industry Applications 8 (2) (2019) 263–270. doi:10.1541/ieejjia.8.263.

[22] K. Åström, P. Hagander, J. Sternby, Zeros of sampled systems, Automatica 20 (1) (1984) 31–38. doi:10.1016/0005-1098(84)90062-1.

[23] R. Kalman, On the general theory of control systems, IFAC Proceedings Volumes 1 (1) (1960) 491–502. doi:10.1016/S1474-6670(17)70094-8.

[24] W. Ohnishi, T. Beauduin, H. Fujimoto, Preactuated Multirate Feedforward Control for Independent Stable Inversion of Unstable Intrinsic and Discretization Zeros, IEEE/ASME Transactions on Mechatronics 24 (2) (2019) 863–871. doi:10.1109/TMECH.2019.2896237.

[25] M. Mae, W. Ohnishi, H. Fujimoto, State Trajectory Generation for MIMO Multirate Feedforward using Singular Value Decomposition and Time Axis Reversal, in: 2019 American Control Conference (ACC), Vol. 2019-July, IEEE, 2019, pp. 5693–5698. doi:10.23919/ACC.2019.8815067.

[26] S. Lang, Linear Algebra, 3rd Edition, Springer, 1987.

[27] R. Pintelon, P. Guillaume, Y. Rolain, J. Schoukens, H. Van Hamme, Parametric identification of transfer functions in the frequency domain-a survey, IEEE Transactions on Automatic Control 39 (11) (1994) 2245–2260. doi:10.1109/9.333769.